Title: Spatial patterns of extracellular enzymes: combining X-ray computed micro-tomography and 2D zymography

Authors: **A. N. Kravchenko[1,2]*, A.K. Guber[1,2], B.S. Razavi[3], J. Koestel[4], E.V. Blagodatskaya[5,6], Y. Kuzyakov[6,7,8]**

[1] Department of Plant, Soil and Microbial Sciences, Michigan State University, East Lansing MI 48824

[2] DOE Great Lakes Bioenergy Research Center, Michigan State University, East Lansing MI 48824

[3] Department of Soil Science and Plant Nutrition, University of Kiel, Kiel, Germany

[4] Swedish University of Agricultural Sciences, Uppsala, Sweden

[5] Department of Soil Ecology, Helmholtz Centre for Environmental Research – UFZ, 06120 Halle (Saale), Germany

[6]Agro-Technological Institute, RUDN University, 117198 Moscow, Russia

[7] Department of Agricultural Soil Science, Department of Soil Science of Temperate Ecosystems, University of Göttingen, Göttingen, Germany

[8] Institute of Physicochemical and Biological Problems in Soil Science, 142290, Pushchino, Russia

*Corresponding author:

Email: kravche1@msu.edu

Phone: (01) 517.353.0469

DOI: 10.1016/j.soilbio.2019.06.002

Abstract

Linking the distribution of enzyme activity to the size and properties of soil pores is a necessary prerequisite for mechanistic understanding of soil biochemical processes. In this study we used soil 2D zymography and X-ray computed tomography (μCT) to assess the relationship between enzymes and pores. The objectives of the study were (i) to assess spatial distribution patterns in the activity of six enzymes contributing to C, N and P cycles, namely, cellobiohydrolase, β-glucosidase, xylanase acid phosphatase, leucine aminopeptidase, and N-acetylglucosaminidase, in soils from five long-term land use and management practices, (ii) to study the correlation between enzyme activities and μCT information, i.e., pore characteristics and image grayscale values, and (iii) to explore the potential use of soil 2D zymography in predicting enzyme activities within 3D soil cores. 3D pore-size distributions were obtained from μCT images of 13 intact soil cores and then 8-15 2D zymography maps were taken from each core. Spatial distributions in the activities of all studied enzymes were auto-correlated; the spatial correlation ranges were equal to ~7-8 mm. The relative activity of all enzymes was positively associated within 60-180 μm Ø pores. Combining 3D μCT information with 2D zymography maps visualized the overall patterns of enzyme activity distributions with respect to soil pores and particulate organic matter locations. Based on the findings we propose a conceptual scheme relating localization of microorganisms, enzymes and substrates to pores of different size ranges. Specifically, we suggest that pores in the tens of microns size range represent optimal microbial habitats, and as such are associated with greater microbial abundance, leading to high enzyme production and activity.

Keywords: Enzyme activities, Spatial statistics, Soil zymography, Pore distribution, Microbial habitats, Microorganisms' localization

1. Introduction

Extracellular enzymes (EEs) produced by roots and microorganisms in order to meet their nutrient and energy demands, play a major role in biochemical processes, including soil organic matter transformations (Burns et al., 2013). Yet, despite substantial efforts in studying EEs, the drivers of their production and subsequent fate in soil are not fully understood (Nannipieri et al., 2012; Burns, 2013). One of the reasons is the extremely high spatial heterogeneity of EE activity (Baldrian, 2014) which can differ by as much as an order of magnitude within a distance of only a few millimeters (Razavi et al., 2016; Ma et al., 2017; Kuzyakov and Razavi, 2019). At a field scale (10 – 100 m), EE spatial patterns are related to patterns in soil fertility (Banerjee et al., 2016), landscape topography (Wickings et al., 2015; Mganga et al., 2016), and land use and management practices (Stursova and Baldrian, 2011; Baldrian, 2014). At a scale of 10 μm – 10 mm, spatial patterns in EE are related to fungal or bacterial colony sizes (Baldrian and Vetrovsky, 2012) and the activity of enzyme producers (Banerjee et al., 2016; Hoang et al., 2016b; Stursova et al., 2016; Navratilova et al., 2017). Hot-spots of EE presence are not only associated with microbial colonies, but also with soil macro- and micro-fauna (Hoang et al., 2016a; Hoang et al., 2016b), plant roots (Razavi et al., 2016; Ge et al., 2017; Razavi et al., 2017) and plant residues (Hoang et al., 2016b; Liu et al., 2017), as well as influxes of fresh organic inputs (Heitkotter and Marschner, 2018). To complicate matters, EEs can react with organic sources and become anchored in the soil matrix while still preserving a certain degree of activity (Nannipieri et al., 2012; Burns, 2013). Moreover, activity of EEs can last surprisingly long after the disappearance of their original microbial producers (Schimel et al., 2017). Quantifying the spatial variability patterns in EE and linking them with those of soil and root characteristics and microorganisms is crucial for understanding what drives EE activities and functions.

The majority of previous studies related EE to soil biological and/or chemical properties as well as to substrate inputs. Chemical and biological processes occur within the physical frame defined by the soil pore network (Young and Crawford, 2004; Or et al., 2007; Tecon and Or, 2017), however, the influences of soil pores on EE have so far been largely overlooked. We hypothesize that variations in soil physical properties, especially the pore presence and characteristics, can also contribute to the distribution of spatial patterns in EEs.

Pores can impact EE distribution within the soil matrix via several mechanisms. They can affect spatial patterns in inputs of the substrates for microbial decomposition directly, i.e., by

driving localization of roots, rhizodeposits, and earthworms (Baldrian et al., 2010a; Baldrian et al., 2010b; Athmann et al., 2017; Banfield et al., 2017a; Banfield et al., 2017b; Navratilova et al., 2017); as well as indirectly, i.e., by influencing diffusion and convective transport of soluble organic compounds (Allison, 2005). Pores can also define micro-environmental conditions, e.g., water regime and O_2 supply (Keiluweit et al., 2016; Keiluweit et al., 2018), which in turn influence the ability of microorganisms to function and produce EEs. Moreover, pores provide the physical space necessary to host microbial colonies, which can range in size from a few dozen to some hundreds of μm (Nunan et al., 2003). The combination of these mechanisms can result in the creation of optimal microbial habitats. Such habitats largely determine the regions of microbial EE production; and higher EE activity can be expected to correspond to these prime habitats.

Visualization of the connections between EE and soil pores could provide valuable input in understanding the *in situ* biochemical processes taking place within an intact soil matrix. One of the possible techniques is coupling soil 2D zymography, which enables EE activity mapping (Razavi et al., 2016), with X-ray computed micro-tomography (μCT), which allows for the 3D characterization of soil pores (Peth et al., 2008; Helliwell et al., 2013). Combining of 3D X-ray μCT information with 2D soil data was pioneered by Hapca et al. (Hapca et al., 2015), who created 3D maps of soil elements' contents using 2D SEM-EDX.

We considered two types of μCT data of potential use in EE spatial variability predictions: (i) the presence and abundance of pores of different sizes and (ii) the grayscale values of μCT soil images. Grayscale values reflect the attenuation of X-rays as they pass through scanned material. The attenuation within solid soil matrix reflect variations in soil mineralogy, presence of pores with sizes below the image resolution, and presence of organic materials, e.g., plant residues and particulate organic matter (POM). They also highlight areas with high soil organic matter (SOM) levels (Kravchenko et al., 2014; Quigley et al., 2018a).

In this study we explored mm-scale, i.e. one to tens of mm, spatial patterns in the distribution of six EEs involved in soil C, N, and P cycling: cellobiohydrolase, β-glucosidase, xylanase, acid phosphatase, leucine aminopeptidase, and N-acetylglucosaminidase (chitinase NAG). Cellobiohydrolase and β-glucosidase are involved in consecutive stages of cellulose degradation (German et al., 2011). Xylanase is responsible for breaking down hemicelluloses (German et al., 2011). Acid phosphatase mineralizes organic P into phosphate by hydrolyzing

phosphoric (mono) ester bonds under acidic conditions (Eivazi and Tabatabai, 1977; Malcolm, 1983; German et al., 2011). Leucine aminopeptidase facilitates hydrolysis of leucine residues from the amino-termini of protein or peptide substrates (Rawlings et al., 2004). N-acetylglucosaminidase (NAG) decomposes chitin to low molecular weight chitooligomer (Baldrian and Stursova, 2011), and decomposes bacterial peptidoglycan. We explored EE activity in soil from several long-term land use and management practices, which over time developed substantial differences in their SOM levels and pore characteristics (Kravchenko et al., 2018).

Our objectives were (i) to assess the spatial variability of the activity of six EEs in intact soil cores, which represent a diverse range of long-term land use and management practices, (ii) to study correlations between EE activity and physical soil properties, i.e., pore characteristics and grayscale values from X-ray μCT scanning, and (iii) to explore the potential of using soil 2D zymography to predict enzyme activity within 3D soil cores with/without μCT information.

2. Materials and methods

2.1. Land use and management systems

The five studied land use and management systems are a part of the Great Lake Bioenergy Center experiment, Kellogg Biological Station, Michigan, USA. The experiment was established in 2008. The soils of the site are well-drained Alfisols of Oshtemo and Kalamazoo series (mesic Typic Hapludalf) (Robertson and Hamilton, 2015). The experimental design is a randomized complete block with five replicated 0.12 ha experimental plots randomly assigned to each land use system. The five studied systems are: continuous corn (*Zea mays* L.) (G1) and continuous corn with winter cover crop of cereal rye (Secale cereale L.) (G2), a monoculture switchgrass (*Panicum virgatum* L.) (G5), a hybrid poplar (*Populus nigra* × *P. maximowiczii* 'NM6') with herbaceous understory (Sprunger and Robertson, 2018) (G8), and an early successional community (G9). Detailed description of the experimental site and management practices can be found at https://lter.kbs.msu.edu/research/long-term-experiments/glbrc-intensive-experiment/ (verified on April 20, 2018). The intact soil cores were collected from the replicated plots of each system from 5-10 cm depth. A total of 13 cores (2-3 cores per system) were used for zymography analyses.

156 *2.2 X-ray µCT scanning and image analysis*

157 Soil pore characteristics and grayscale values were obtained via X-ray µCT image
158 analyses. For that, the soil cores were subjected to X-ray scanning using a GE Phoenix v|tome|x
159 at the Institute of Soil and Environment at the Swedish University of Agricultural Sciences in
160 Uppsala. 3D µCT X-ray images were reconstructed using the GE software datos|x. Detailed
161 description of the scanning specifications is reported in Kravchenko et al. (2018). Each image
162 had a resolution 29 µm in all directions.

163 The image processing was conducted in ImageJ/Fiji software (Schindelin et al., 2012).
164 Preprocessing consisted of a 3D median filtering with a radius of two in all directions to reduce
165 random noise. We removed 0.5 cm border part around each core to avoid artifacts associated
166 with sample wall effects. Based on the scanning resolution of µCT analysis, we identified pores
167 with diameters >60 µm, referred to as visible pores. The thresholds were computed using
168 minimum error thresholding approach (Kittler and Illingworth, 1986). Following (Nakagawa and
169 Rosenfeld, 1979) the two-Gaussian fits were applied to sequences of grayscale histograms of 2D
170 images separately for each soil core. For these computations we used the Regression Wizard tool
171 of the SigmaPlot software (Systat Software, Inc). Then, pore size distributions were obtained
172 using the Pore size distribution tool of Xlib plugin for ImageJ, based on the maximum inscribed
173 spheres approach (Munch and Holzer, 2008). On the studied images we also identified fragments
174 of particulate organic matter using the approach outlined in Kravchenko et al (2014).

175 Another employed µCT image characteristic was µCT grayscale values of the soil solid
176 matrix voxels. The grayscale values reflect the attenuation of X-rays as they pass through the soil
177 sample; they are driven by the density of the material and by the atomic numbers of the
178 constituting elements (Ketcham, 2005; Peth, 2010). On 8-bit images, the voxels that contain
179 primarily pore space (air) appear dark and have grayscale values close to zero, while the voxels
180 that contain primarily solid material dominated by elements with high atomic number, e.g., iron,
181 appear bright and have grayscale values close to 255. Here we only used the grayscale values of
182 the image voxels that were classified as solids; the gray scale values from the image voxels that
183 were classified as pores were not used in this analysis. Thus, the darker grayscale values of the
184 studied solid voxels correspond to the greater abundance of elements with low atomic numbers,
185 notably, carbon (Quigley et al., 2018b). Please note that darker values could also be related to
186 greater presence of pores smaller than the scanning resolution (<60 µm Ø pores).

187

188 *2.3. 2D zymography of soil core slices*

189 Mapping of soil enzyme activities was conducted via 2D soil zymography (Spohn and
190 Kuzyakov, 2014; Razavi et al., 2016), as described in detail in Razavi et al (Razavi et al., 2016).
191 In a course of 2D zymography a membrane saturated with an enzyme-specific substrate is placed
192 on a soil surface. Contact between substrate and enzyme releases a fluorescent product (e.g.
193 MUF: methylumbelliferon, AMC: 7-amido-4-methylcoumarin) and the resulting fluorescing
194 patterns reflect spatial distribution of active EE (Guber et al., 2018).

195 Hydrophilic polyamide filters (0.45 µm pore size; 100 µm thick, Tao Yuan, China) were
196 used as membranes (Razavi et al., 2016; Sanaullah et al., 2016). Photos of the membrane on the
197 soil surface were taken using Nikon D90 camera (Nikon Inc.) with a Sigma 18-250 mm f/3.5-6.3
198 DC Macro OS HSM lens (Sigma Corp. of America) installed on a Rocwing Pro Copy Stand
199 (Rocwing Co., UK). The source of UV light was a 22W Blue Fluorescent Circline Lamp -
200 FC8T9/BLB/RS (Damar Worldwide 4 LLC.).

201 Six enzymes were studied: β-glucosidase, cellobiohydrolase, xylanase, N-acetyl-beta-
202 glucosaminidase (chitinase, NAG), leucine aminopeptidase, and acid phosphomonoesterase Acid
203 phosphatase). The respective enzyme-specific substrates used were: 4-Methylumbelliferyl-β-D-
204 Glucoside, 4-Methylumbelliferyl-β-D-Cellobioside, 4-Methylumbelliferyl-β-D-Xylopyranoside,
205 4-Methylumbelliferyl-N-Acetyl-β-D-Glucosaminide, L-leucine-7-amido-4-methylcoumarin
206 hydrochloride, and 4-methylumbelliferyl-phosphate (Razavi et al., 2017). Each substrate was
207 dissolved in a concentration of 6 mM in either TRIZMA buffer (was used for AMC-based
208 substrate - leucine aminopeptidase, pH: 7.2) or MES (2-(N-morpholino)ethanesulfonic acid)
209 buffer (was used for MUF-based substrates - all other enzymes, pH: 6.5): [MES(pH: 6.5)
210 ($C_6H_{13}NO_4SNa_{0.5}$) TRIZMA (pH: 7.2) ($C_4H_{11}NO_3$•HCl, $C_4H_{11}NO_3$] (Razavi et al., 2017).

211 We obtained 8-13 enzyme maps per each intact soil core (1-3 maps of each individual
212 enzyme from each core) for a total of 180 enzyme maps. One enzyme map was obtained per each
213 soil slice. The order in which specific enzymes were measured within the core was randomized.
214 For the measurements, each core was placed within a cutting table (Supplement Fig. 1). A
215 calibrated handle at the bottom of the table allowed pushing the core out of the sample cylinder
216 in 0.5 mm increments. At each 0.5 mm increment the soil layer pushed above the table was
217 removed manually using a microtome knife. Care was taken to minimize disturbance to the soil

surface while cutting, by removing stones or large sand grains with tweezers from the surface prior/during cutting. Enzyme maps were obtained on soil surfaces in 2 mm increments (Supplement Fig. 1). For that, a polyamide membrane (Ø 4.5 cm) was saturated in 240 µl of the MUF/AMC-based substrate solution and placed on top of the prepared soil surface. Additional 120 µl of the substrate solution was added on top of the membrane with a pipette and evenly spread with a fine brush. The membrane was covered by a layer of aluminum foil followed by a 100 g sandbag weight. The membrane was incubated on the soil surface for 30 minutes at room temperature, then it was placed within a light-proof zymography chamber and a photo was taken in UV light as described above. The membrane was then removed from the soil surface.

Because of unevenness of the soil surface, only a portion of it was in full contact with the membrane; thus reliable enzyme activity data could be obtained only from the portions of the membrane (Guber et al., 2018). In order to estimate presence and strength of the contact we used MUF-staining approach (Guber et al., 2018b). For that, immediately after removing the membrane with the substrate, we applied to the soil surface a membrane fully saturated with 6 mM MUF solution. The membrane was covered with a 100 g sandbag and kept for 30 s. Then, the soil surface was photographed in UV light. The bright areas on the image indicated the localities on the soil surface that received MUF from the membrane, and thus could be regarded as such that were in contact with the membrane. The image processing was conducted in ImageJ and the images were converted into an 8-bit format. The image from the substrate membrane was matched with the image of the MUF-stained surface, and the areas with minimal contact, that is, with MUF-stained grayscale values of <30 (0-255 grayscale scale), were excluded from further enzyme map analyses.

2.4. Matching enzyme maps with µCT information

The enzyme maps were obtained from the surfaces of the individual soil slices (Supplement Fig.1b). The enzyme map was covered by a 1 mm^2 grid and EE readings from zymograms were used to produce as single value per each 1 mm^2 grid cell. For that, for each 1 mm^2 pixel of the enzyme map we, first, calculated the average grayscale value corresponding to it, then, the pixel averages were further standardized based on the mean and standard deviations of the entire map. The latter step was necessary to enable comparisons among different enzymes and systems.

249 Then, for each soil slice we identified the corresponding layer from the μCT image, such
250 that the center of the layer corresponded to the soil slice (Supplement Fig. 1c). The μCT layers
251 were 1 mm in height, 0.5 mm above and below the soil surface layer. The μCT information was
252 aggregated to 1 mm^3 grid cells. For each 1 mm^3 grid cell we calculated the total volumes of the
253 pores of the studied sizes. For example, for each given 1 mm^3 grid cell we had the number of 29-
254 μm voxels of the original μCT image that belonged to that cell and that were occupied by 60 μm
255 diameter pores, and that number was used to calculate the volume of the 60 μm pores in that grid
256 cell. The gray scale values from all 29-μm voxels of the original μCT image that belonged to that
257 1 mm^3 cell were used to calculate the average gray scale value of the cell.
258 To match enzyme maps from soil slices with 3D information from μCT scans
259 horizontally, we used the mark placed on an acrylic tube of each soil core prior to μCT scanning.
260 The cores were located within the cutting table so as to ensure a match between the mark and the
261 position of the zymography membrane on the soil surface. To match them vertically, we used
262 visual observations from the 3D images and pictures of soil surface taken at each soil cut, and the
263 height of the soil remaining after all the desired enzyme slices were cut from the soil core.
264 The aggregation of the data to the 1 mm scale conducted here was a conservative
265 measure to address the uncertainties associated with some movement of soil during surface
266 cutting as well as with matching enzyme maps with μCT images. However, it did introduce
267 smoothing into the resulting pore data.
268
269 *2.5. Data analysis*
270 Removal of artificial spatial trends
271 Despite the best efforts, during placing the substrate membranes on the soil surface there
272 was some unevenness in the redistribution of the liquid substrate through the membrane. These
273 spatial trends could distort the assessments of spatial variability patterns via variography. To
274 ensure that such redistribution is not affecting the variogram estimates we removed the trends
275 using multiple regression models. Application of polynomial models with various degrees of
276 complexity was explored and the model that appeared to adequately describe the spatial trend in
277 most of the studied 180 samples was the model with linear effects of x and y spatial coordinates.
278 Specifically, for each enzyme map we fitted the regression model to the EE data, obtained

residuals from the regression analysis, and then used the residuals in all further analyses as a measure of relative EE activity corrected for presence of linear spatial trends.

Variography

Sample variograms of the residuals, obtained from the trend removal procedures described above, were calculated individually for each 2D enzyme map. We used lag distance of 1 mm and considered 30 lag distances, thus, covered 30 mm of the sample, avoiding border effects. The number of point pairs in the considered lags always exceeded 500, hence was sufficient for a reliable estimation of the sample variogram value (Goovaerts, 1998). Variogram calculations were conducted using PROC VARIOGRAM in SAS (SAS 9.4).

The spherical model was used in variogram fitting for kriging, as the model that was adequately fitting most of the obtained sample variograms. Automated fitting of all 180 sample variograms was not possible because of convergence problems, thus manual fitting was performed. As a nugget, we selected the sample variogram value at the first lag; and the sill was "eye-ball" selected as the value corresponding to the plateau. The spatial auto-correlation range was set as the lag distance corresponding to the sill. As a measure of proportion of the variability occurring at distances < 1,000 μm we used the ratio of nugget and sill (N/S) expressed as percent.

Ordinary and regression kriging

Prediction accuracy of 2D zymography data was tested using test-model data set approach (Goovaerts, 1998). That is, the data were divided into two sub-sets, a model data set and a test data set. The model data set was used for generating kriging predictions for the test data set. The test data set consisted of a total of 120 randomly selected data points (Supplement Fig 2). The remaining data constituted the model data set. We used data from all individual 2D enzyme maps sequentially

For ordinary kriging (OK), the model data set was used to compute a sample variogram and determine the variogram model parameters, as described above. Then, the model parameters were used in 2D OK to generate predictions for the test data points. SAS procedure PROC KRIGE2D was used to perform OK. The search radius was set to 14 mm and the minimum and maximum number of data points used in kriging estimation was set to 4 and 10, respectively. For

regression kriging (RK), the model data set was first used to relate EE values with auxiliary variables from μCT images, i.e., abundances of pores of different sizes and grayscale values. Predicted values for the test data points were recorded. Then the residuals from the fitted model were used in computing sample variogram, fitting variogram model, and obtaining kriging predictions at the test data points. The final predictions for each test data point were obtained by adding predictions from the linear regression model and the kriging predicted residuals. For both OK and RK the correspondence between true and predicted values for the test data sets were assessed using R^2 values, MSE, along with parameters (slope and intercept) of the regression equation relating true values with predictions.

Statistical analysis

Statistical analyses, ANOVA and ANCOVA, were conducted in SAS using PROC MIXED and PROC GLIMMIX tools (Milliken and Johnson, 2001, 2009). Statistical models for exploring spatial parameters for the studied enzymes included the fixed effects of the enzymes and the land use systems and the interaction between them, and the random effects of blocks, plots, and cores (nested within systems and plots). Normality of the residuals and homogeneity of variances were checked for each variable. In case of marked deviations from normality the data were log-transformed, while in case of variance heterogeneity, unequal variance analysis was performed (Milliken and Johnson, 2001, 2009). Significant interactions were examined using analysis of simple effects, and, when significant, were followed by multiple comparisons via t-tests. The results are reported as statistically significant at 0.05 level.

To assess the associations between EE and auxiliary variables from μCT images, correlation analysis and ANCOVA were applied. For ANCOVA we used the statistical model described above and added to it the linear effects of the auxiliary variables of interest. The resulting linear coefficients were then used to explore the patterns in relationships among six EE in the studied land use systems. To facilitate comparisons we report standardized coefficients from these analyses, i.e., *t*-values.

3. Results

3.1. Spatial variability patterns

340 Spatial autocorrelation was present in the activity distributions in all soil slices from all
341 studied EE and land use systems. Examples of β-glucosidase and acid phosphatase maps of EE
342 activity are shown on Fig. 1 along with the corresponding sample variograms fitted with
343 spherical models.
344 ANOVA indicated no interactions between EE and land use systems and no land use
345 effects ($p>0.05$) (Supplement Table 1), thus we focused the analyses on the main effect of EE.
346 Acid phosphatase and leucine aminopeptidase had much higher nuggets and sills than the other
347 EE (Fig. 2a and b), indicating an overall greater variability in their activity. However, their N/S
348 ratios were lower than for the other enzymes. The N/S ratio was 47% for acid phosphatase and
349 54% for leucine aminopeptidase, for other EE it exceeded 60%. Since N/S ratios here represent
350 the proportion of the random variability occurring at distances <1000 μm, the lower values in
351 phosphatase and leucine aminopeptidase suggest that the distribution patterns of these enzymes
352 had greater spatial continuity than that of the other EE, while small random patches were more
353 abundant in the other EE's distributions. Overall, N/S ratios were quite substantial and ranged
354 from 17% to 80% in individual soil slices. The average spatial correlation range across all
355 enzymes and land use systems was equal to 7.5 mm; no significant differences among the
356 enzymes and among systems were observed.
357
358 *3.2. Correlations of EE activities with X-ray μCT information*
359 In most soil slices the studied EE were negatively correlated to grayscale values from X-
360 ray μCT images (Fig. 3). NAG and β-glucosidase were the two enzymes with the strongest
361 associations with the grayscale values (Fig. 3). For the other two enzymes involved in C cycle,
362 i.e., cellobiohydrolase and xylonase, the associations with the grayscale values were relatively
363 weak. With the exception of a few slices, acid phosphatase was not correlated with grayscale
364 values.
365 Associations with pores of various sizes varied among the six enzymes, but positive
366 relationships with 60-180 μm Ø pores and subsequent decrease with further increasing pore sizes
367 was present in all EEs (Fig. 4). For 60 μm pores, the associations were the highest for β-
368 glucosidase, closely followed by acid phosphatase, and then by NAG. Associations with 120 μm
369 pores were the strongest for phosphatase, followed by β-glucosidase, and NAG. Associations

with pores of 180-300 μm size range were substantially stronger for acid phosphatase as compared to the other EEs. All enzymes were negatively associated with pores 360 μm (Fig. 4).

3.3. Kriging predictions

As expected, the R^2 values for test data set predictions were higher (Fig. 5) for the enzymes with greater spatial autocorrelation, i.e., acid phosphatase and leucine aminopeptidase. The R^2 values for these two enzymes were around 0.45, while for the other enzymes they were in 0.30-0.35 range. Adding auxiliary X-ray information, i.e., grayscale values did not lead to a substantial improvement in mapping accuracy during regression kriging (results not shown).

4. Discussion

Our findings can be interpreted at two spatial scales: tens-of-mm spatial scale for the EE spatial variability data and tens-of-micron scale for correlations between EE and μCT data. Note that the soil cores here were investigated in the absence of live plant roots, thus the observed relationships can be regarded as typical for a soil matrix outside of the actively functioning rhizosphere. Despite our expectations, the spatial distributions of EE activities and their associations with pores did not differ among the studied land use systems.

4.1. Spatial variability patterns of enzyme activities

Spatial distributions of EE activity at tens-of-mm spatial scale were auto-correlated (Fig. 2), but between 47% and 60% of EE variability took place at distances <1000 μm. The strengths of spatial auto-correlation in distribution of EE at the studied spatial scale are likely related to: (i) spatial patterns of EE's microbial producers, and (ii) spatial patterns and diffusion rates of the substrates subject to the enzymes. In the absence of live roots, microbial activities are the main driver of EE production (Nannipieri et al., 2012; Burns, 2013). However, past history, such as former presence and activity of live plant roots, affected the spatial distribution patterns of both microorganisms and EE substrates.

Even though the spatial resolution of our study was too coarse to conduct in-depth assessment of the spatial patterns in microbial producers, the highly patchy distributions of enzymes observed here are consistent with the typically reported, very sparse distributions of microorganisms (Nunan et al., 2003; Franklin and Mills, 2009; Baldrian and Vetrovsky, 2012).

Presence of bacterial colonies and individual cells are highly sporadic even on plant roots, which are the sites of the greatest microbial activity in soils (Schmidt and Eickhorst, 2013). The typical reported sizes of microbial colonies and spatial correlation ranges in their distributions are much smaller than the studied resolution (1000 μm). For example, Nunan et al. (Nunan et al., 2002; Nunan et al., 2003; Nunan et al., 2006) reported 100-600 μm spatial correlation ranges for bacteria presence. Probandt et al. (Probandt et al., 2018) observed that the average distances between individual bacteria cells on sand grains varied from 0 to 29 μm. It can be surmised that sporadic patterns in microbial distributions played a major role in EE variability and were responsible for the high spatially unexplained component in the EE variograms.

Spatial patterns and diffusion rates of EE substrates were the other possible source of the observed auto-correlations. Specifically, comparisons among the studied EE enabled insights into how differences in their substrates can be the potential source of the observed differences in EE spatial patterns. For example, lower N/S ratios for leucine aminopeptidase and acid phosphatase as compared to the other EE could be related to the fact that they have relatively low substrate specificity and can act on different substrates including a variety of compounds within non-particulate SOM (Alef et al., 1995). These enzymes can be expressed by a wide range of producers (Dick and Tabatabai, 1984; Blagodatskaya and Kuzyakov, 2008; Nannipieri et al., 2012). Also, it is assumed that the mobilization of organic P by phosphatases is necessary over larger soil volumes compared to the enzymes responsible for other nutrients (Kuzyakov and Razavi, 2019), because P delivery to roots is strongly controlled by diffusion, which is very slow for P (Nye and Tinker, 1977). Mancarella et al (Mancarella et al., 1981) suggested that the soluble form of aminopeptidase in soil is a result of proteolytic and non-proteolytic processing of epithelial cell membranes and that it is not a true secretory product. This is also valid for intercellular phosphatase which can be released from the cells of plants, fungi and bacteria after lyses, and can react as EE in soil matrix. However, the substrates for the other studied enzymes are primarily plant and fungal residues and spatial continuity in their distribution patterns is typically quite low. This makes their distribution random and sporadic, which would explain the observed differences in enzyme auto-correlations.

Differences between β-glucosidase and cellobiohydrolase in the strength of association with pores, namely, strong positive correlation for β-glucosidase and relatively weak correlations for cellobiohydrolase, might be an indication of the importance of substrate diffusion rates. Even

though β-glucosidase and cellobiohydrolase are both involved in cellulose degradation (Nannipieri et al., 2012), the substrate of cellobiohydrolase activity is insoluble cellulose while the substrates of β-glucosidase are soluble compounds, e.g. disaccharides (Alef and Nannipieri, 1995). The latter can easily diffuse within the soil matrix, with pores being the avenues for such diffusion. The spatial patterns in *β*-glucosidase likely follow the spatial patterns of its soluble substrates which are then reflected in positive correlations of *β*-glucosidase activities with pores. Work by Bailey et al. (2017) demonstrated that fine pores with ~6 μm neck diameters contained more complex organic compounds than large pores with ~200 μm necks, while large pores had greater presence of simple soluble organic. Note that the enzymes diffusion is negligible (Guber et al., 2018), thus, the reactions between enzymes and substrates are driven solely by substrate diffusion and substrate mass flow with water.

4.2. Associations with pores

Even though the pore size distribution data were aggregated to 1 mm spatial scale, the EE associations with pores of different sizes are indicative of the processes taking place at tens-of-micron scale, i.e., the scale corresponding to μCT resolution. Presence of most enzymes was positively associated with 60-180 μm pores, while negatively associated with presence of 360 μm pores (Fig. 4). Positive associations of EE with 60-180 μm Ø pores (Fig. 4) are consistent with a substantial body of experimental evidence suggesting that such pores are of particular significance for soil microbial functioning.

We suggest that pores of this size range are optimal microbial habitats, and as such are associated with greater microbial abundance, leading to high enzyme production and activity (Fig. 6). For once, the micro-environmental conditions within these pores are better for microbial functioning than those in pores of other sizes. Pores of this range are associated with greater presence of fine roots (Pagliai and Denobili, 1993), and thus with greater new C inputs (Quigley et al., 2018a). These pores are also the main transport avenues for soluble organic substances released by litter decomposition (e.g. in O horizon) and/or from detritusphere. Pores of this size range likely provide optimal water availability and do not often experience a lack of O_2 (Keiluweit et al., 2017). These pores probably also supply an optimally-sized physical space for the formation of active microbial colonies, since pores of <10 μm Ø are too small to furnish sufficient space for colony formation. Better micro-environmental conditions likely lead to more

active microbial communities populating these pores. Wright et al., (1995) reported higher activity of bacteria introduced into 6-30 μm as opposed to small (<6 μm) pores. Carbon newly added to soil via plant roots is most actively consumed in pores of this size range (Quigley et al., 2018a). They are the locations of faster C turnover and greater decomposition of newly added organics (Strong et al., 2004; Ruamps et al., 2011; Ruamps et al., 2013). Dissolved organic carbon extracted from pores of this size group was found to be more recalcitrant than that from < 10 μm pores, suggesting quick consumption of labile compounds by resident microbes (Bailey et al., 2017). Indeed, these pores were found to differ in terms of their microbial community composition (Ruamps et al., 2011; Ruamps et al., 2013).

Based on their C inputs, micro-environmental conditions, and size, the tens-of-μm pores constitute prime microbial habitats (Fig. 6) and are, potentially, the areas with the greatest microbial presence and activity within the non-rhizosphere soil matrix. Higher EE activity associated with greater abundance of such pores (Fig. 4) in all tested enzymes supports the prime microbial habitat theory.

Enzyme mapping

While the observed associations are providing new insights into factors driving spatial patterns in EEs distributions within intact soil matrix at few mm spatial scale, the strength of the observed relationships was not sufficient to achieve high accuracy for EE micro-scale mapping. The biggest roadblock was an extremely high variability of EE' activity at <1000 μm distances. N/S ratios, which are the quantitative representations of that variability, exceeded 50% in most soil slices and were as high as 80% in some of them. Nevertheless, the R^2 values obtained from ordinary kriging were in a 35-45% range (Fig. 5a). The stronger spatial autocorrelation, as in acid phosphatase and leucine aminopeptidase distributions, the higher accuracy in kriging maps.

Correlations of EE activities with X-ray μCT data, while statistically significant, and meaningful from biogeochemical standpoint, numerically were relatively weak. In cases when the auxiliary variable is only weakly correlated to the main variable of interest the incorporation of the auxiliary information via either regression kriging or co-kriging typically does not lead to sizeable improvement in accuracy. For example, a reliable improvement in prediction accuracy via regression kriging was only possible when the R^2 for the linear regression between the main and auxiliary variables exceeded 0.6 (Zhu and Lin, 2010), the condition that was barely present

among the soil zymography slices. Even when the R^2 values are relatively high, the improvement in mapping accuracy due to regression kriging may still be only minor if spatial autocorrelations of the main and auxiliary variables are interrelated (Kravchenko and Robertson, 2007).

The mentioned above very high patchiness in microbial community locations and activities (Nunan et al., 2002; Franklin and Mills, 2009; Baldrian and Vetrovsky, 2012) suggests that only predictions and mapping at scales less than a hundred micron would be able to explain significant portion of EE variability. In this study the resolution of the μCT data was 30 μm. The resolution of zymograms is not possible to establish precisely due to the diffusion of products of enzyme catalysis (Guber et al., 2018b), but an estimate of 100 μm seems plausible. Yet, because of the inaccuracies potentially involved in matching the two sources, the 1000 μm resolution for the final joint data sets combining zymography and μCT was the only reasonable option for this study.

Even though the predictions of specific locations of EE activity were not possible, the approach did offer the possibility of exploring general associations between EEs and characteristics of soil micro-environments with potential relevance to EE distributions as well as their visualizations (Fig. 5b, Supplemental video 1).

In further work, greater reduction of uncertainties in spatial coupling of the two data sources can be achieved by improving zymography and X-ray μCT image matches (Guber et al., 2018a). The high random component in spatial patterns of soil microorganisms, i.e. sources of EE in the soil, suggests that additional factors/drivers, e.g., fresh C inputs, variations in pH and soil moisture, need to be considered and better matching approaches are necessary for improvements at the finer spatial resolutions.

5. Conclusions

At the studied scales of a few mm, within non-rhizosphere soil matrix, we found spatial autocorrelations in distributions of all studied EE. Observed spatial patterns are a function of spatial patterns in the distributions of microbial producers, but also of nature, availability, and diffusion properties of EE substrates.

Positive associations between pores with 60-180 μm diameters and relative EE activities were found for all studied enzymes, across all five studied land use and management practices. Apparently, micro-scale areas with prevalence of such pores experience elevated levels of

525 microbial activities leading to EE production and are the potential hotspots of C, N and P
526 cycling. The results suggest that in the studied soils pores of this size range serve as a prime
527 habitat for soil microbial communities.
528

529 **Acknowledgements**

530 This work was funded in part by National Science Foundation's Long-Term Ecological Research
531 Program (DEB1027253) and by the National Science Foundation's Geobiology Program
532 (Award #1630399). This study is supported by the US Department of Energy, Office of Science,
533 Office of Biological and Environmental Research, under Award Number DE-SC0018409, by the
534 DOE Great Lakes Bioenergy Research Center (DOE BER Office of Science DE - FC02 -
535 07ER64494), and by USDA (MICL02600). The work of A. Kravchenko was supported by
536 DAAD - German Academic Exchange Service's program "Research Stays for University
537 Academics and Scientists, 2017" (57314018) and by the Research Award from the Alexander
538 von Humboldt Foundation. Contribution of E. Blagodatskaya was motivated and supported
539 within the framework of the priority program 2089, funded by the DFG (German Research
540 Foundation) - Project # 403664478. Contribution of Y. Kuzyakov was supported by the Russian
541 Science Foundation (project No. 18-14-00362).
542

Figure 1. Examples of zymograms for β-glucosidase (top) and acid phosphatase (bottom) and their corresponding variograms of detrended values for one of the studied soil cores. Color gradient represent the range of enzyme activity from low (blue) to high (yellow). White scale bar represents 1 cm. Vertical lines mark spatial correlation ranges.

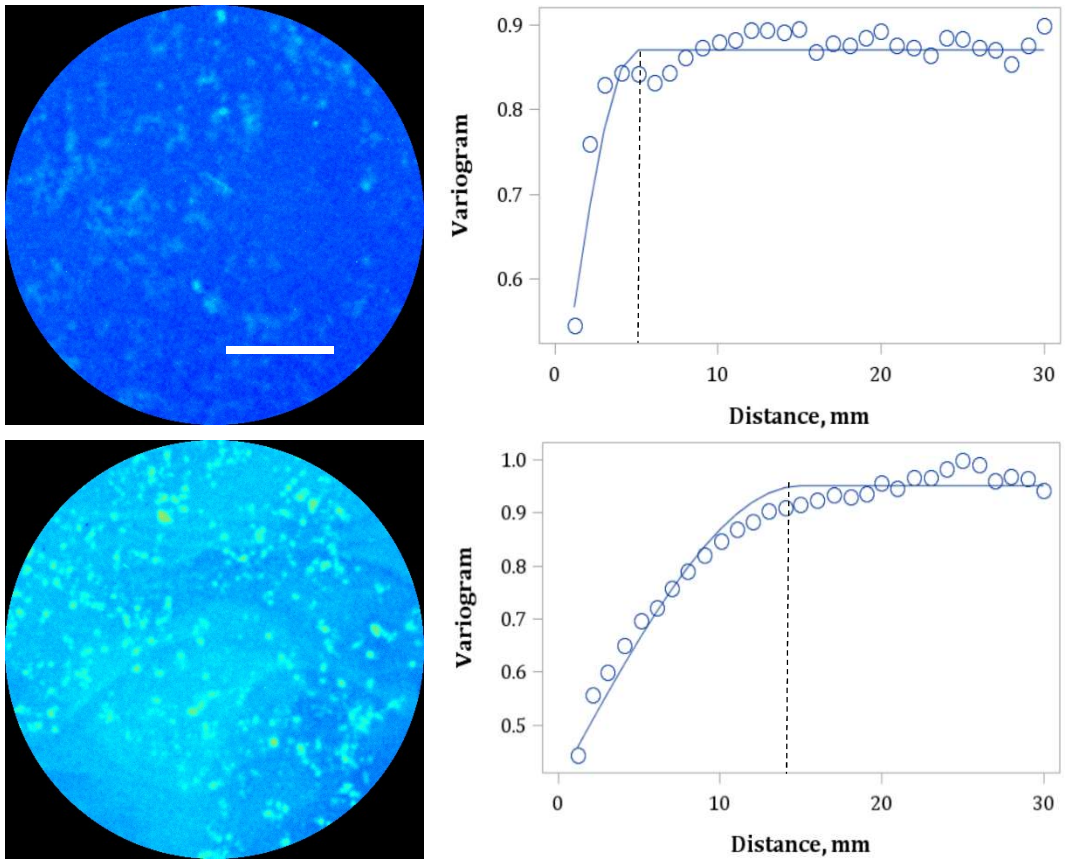

Figure 2. Nuggets (a), sills (b), and N/S ratios (c) for the studied enzymes across all land use systems. Shown are means and standard errors. Letters mark significant differences (at $p < 0.05$).

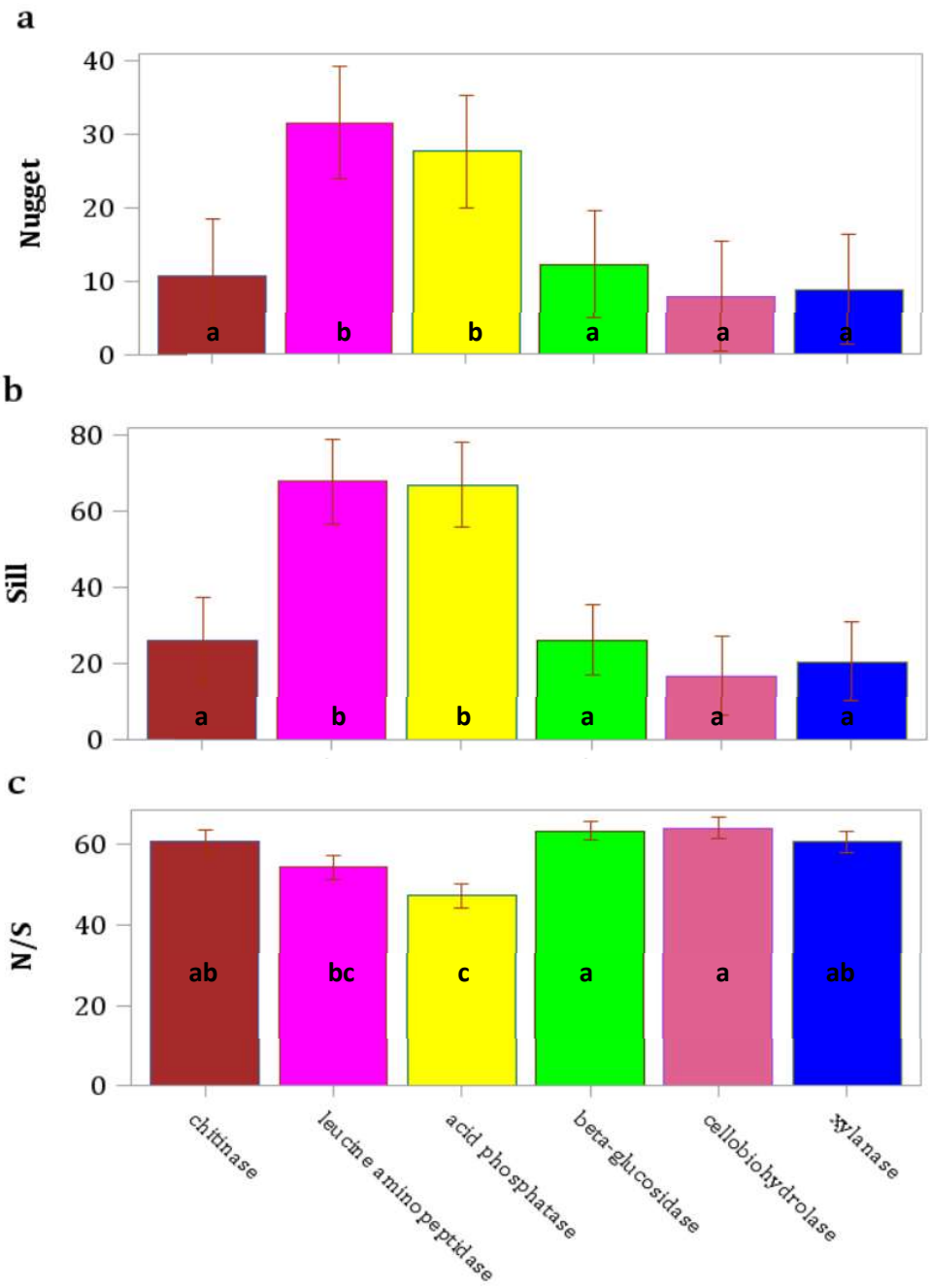

Figure 3. Correlation coefficients between µCT grayscale values from solid voxels and standardized values of the studied six enzymes. Horizontal lines and dots within the boxes mark medians and means, respectively, while outside dots mark outliers. Shaded area marks correlation coefficients that are not significantly different from zero ($p<0.05$). Note that negative correlations signify that higher EE levels were present in darker (lower grayscale value) areas of µCT images, which are in part associated with greater presence of organic materials.

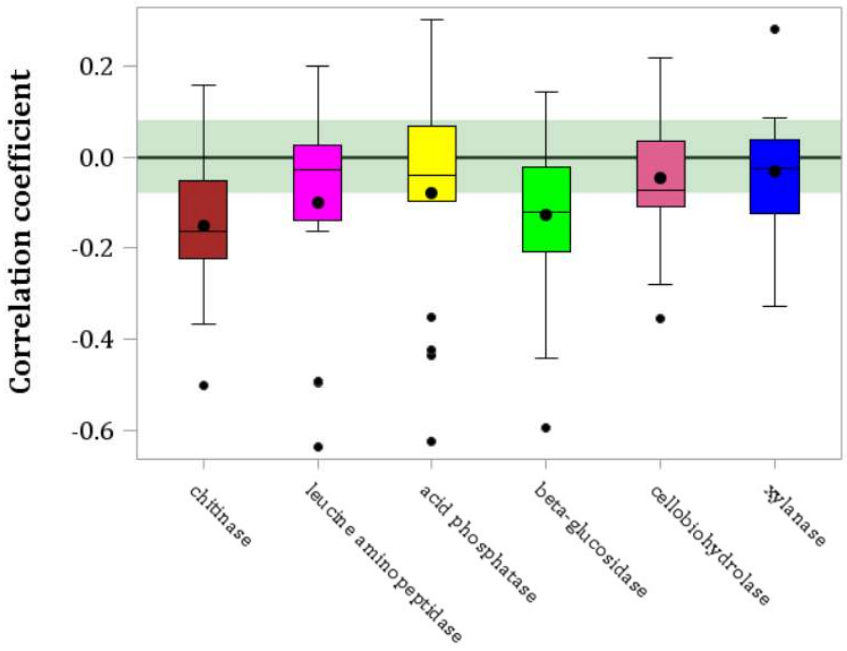

Figure 4. Standardized linear regression slopes from ANCOVA relating enzyme activity with volumes of pores of different sizes across all studied sites. Shaded area marks correlation coefficients that are not significantly different from zero ($p<0.05$).

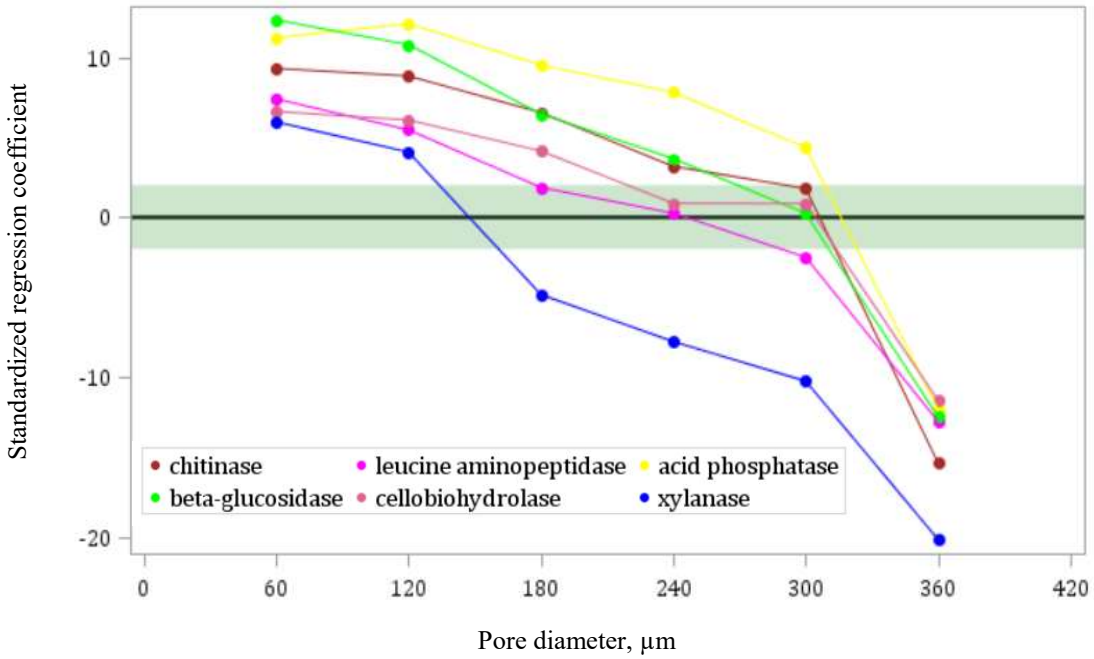

Figure 5. (A) R^2 values from predicting test data set values using ordinary kriging. A total of 120 randomly selected observations from the independent test data set are predicted in every soil slice. Letters mark significant differences among the enzymes (at $p < 0.05$). (B) A section of a 3D map of β-glucosidase (pink) distribution within an intact soil core obtained from regression kriging along with soil pores (blue) and particulate organic matter (green). White scale bar represents 5 mm.

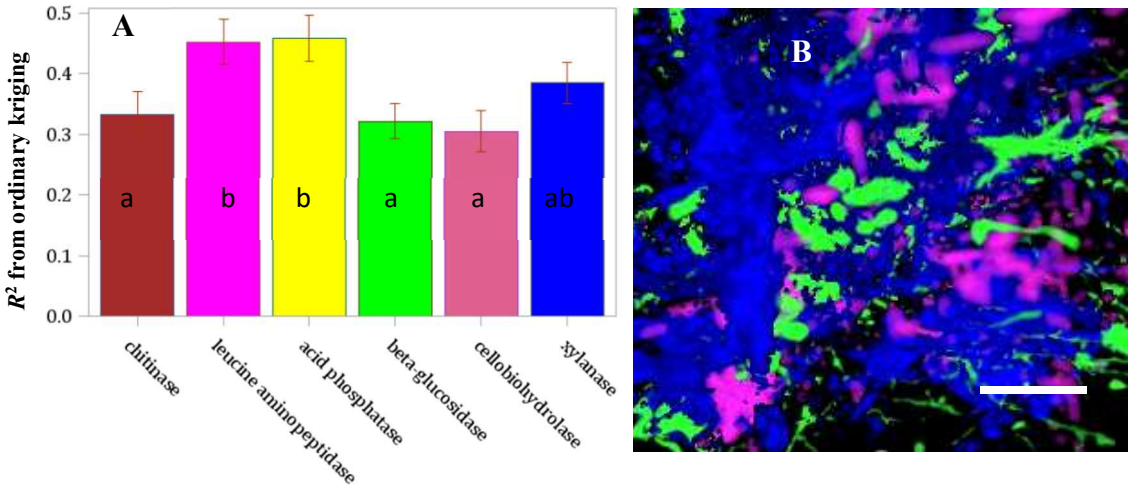

Figure 6. Hypothesized relationships between extracellular enzyme (EE) activities, abundance of microorganisms, new carbon inputs from root exudates, and availability of water and O_2 in pores of different sizes. The highest EE activity corresponds to the optimum between water and O_2 availability and high level of root exudation. Low EE activity in pores <10 µm is also related to these pores being too small to maintain sizeable microbial colonies, while pores > 300 µm are too large to provide 3D connectivity between colonies located on the pore surfaces and too accessible for grazing by the predators.

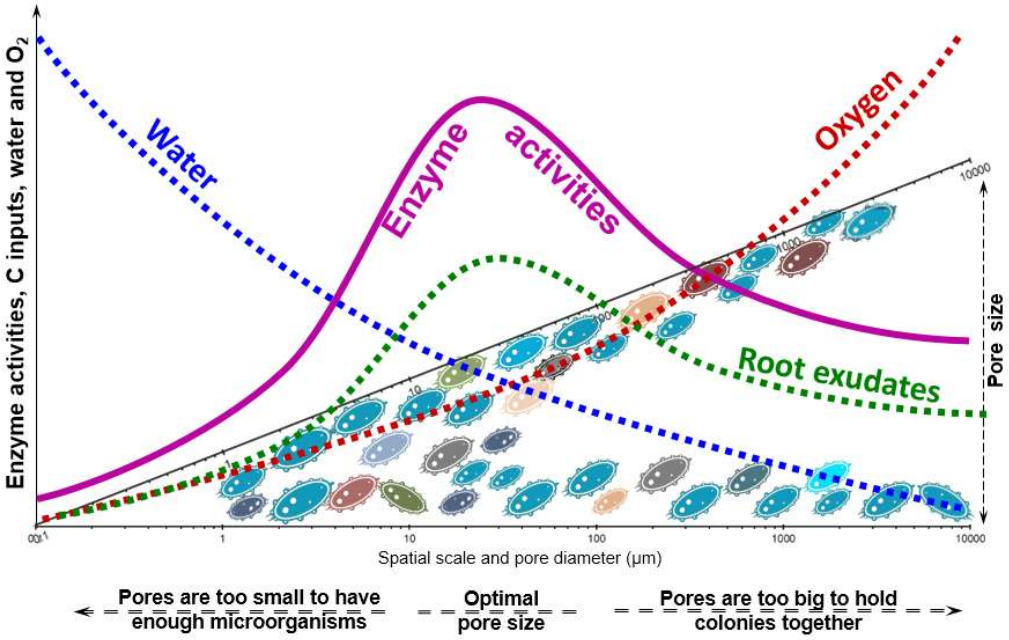

Appendix

Supplement Figure 1. Intact soil core within a cutting table: a view from the top (a) and a view from a side with a 2 mm soil layer pushed out using the calibrated handle below (b); and schematic representation of the soil cutting and subsequent matching of soil surface slices where zymography was conducted with corresponding 1mm deep layer of µCT image data (c).

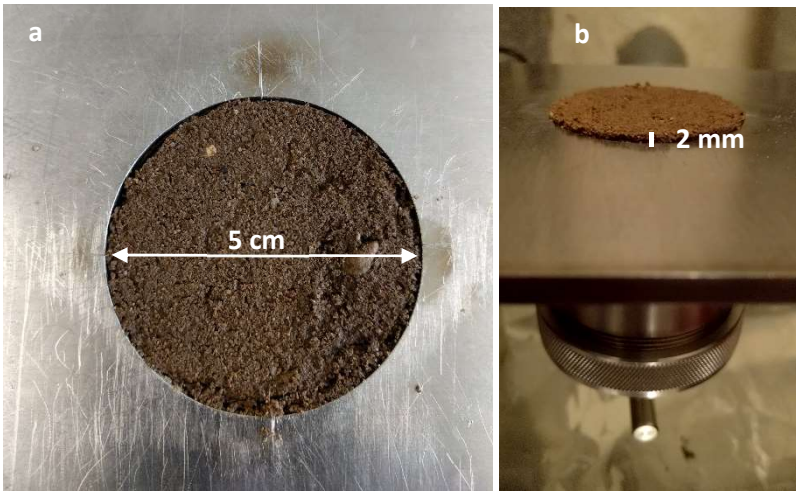

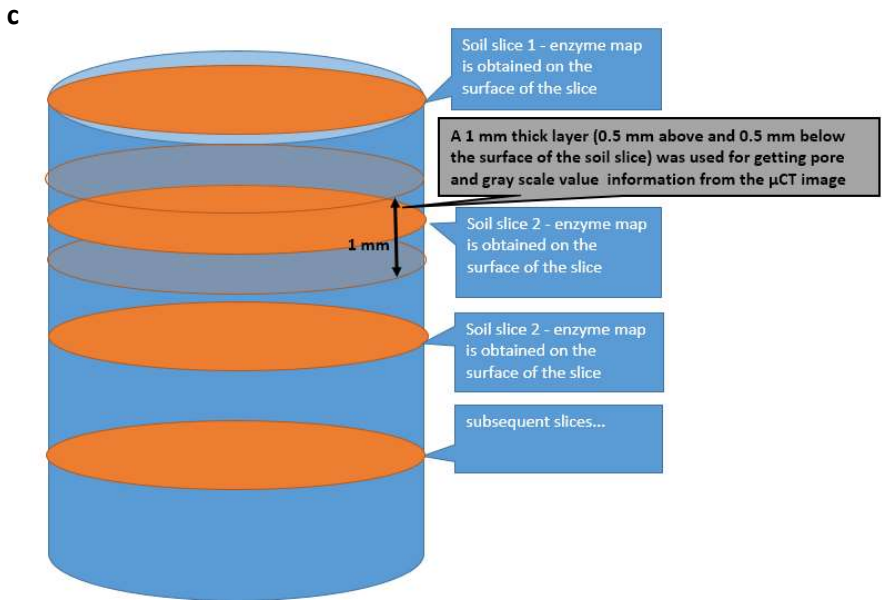

Supplement Figure 2. An illustration of a data from one soil slice used in assessing accuracy of kriging mapping. The black circles are the locations of the data points that were used for mapping (model data set) and the green circles are the locations to be predicted (test data set).

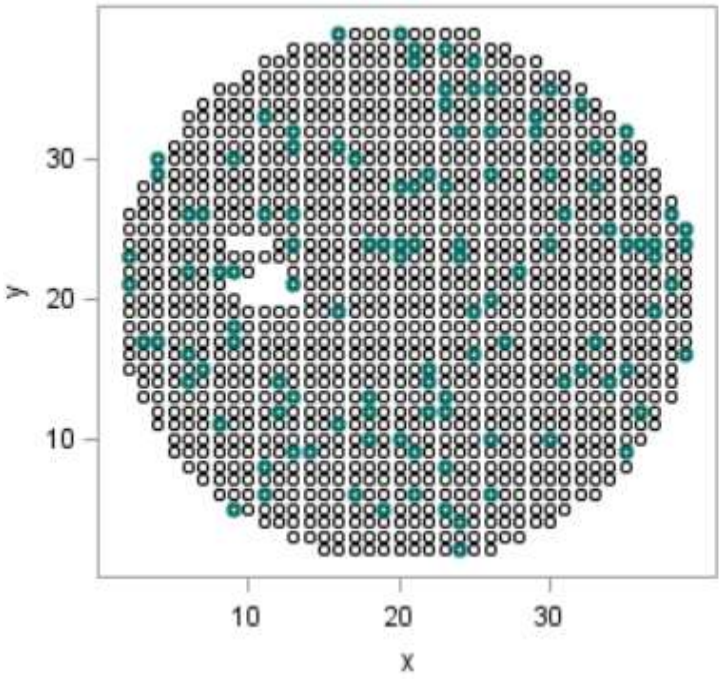

Supplement Table 1. Results of ANOVA for the effects of the land use systems, enzymes, and system by enzyme interactions on geostatistical parameters, namely, nugget, sill, range, and nugget-to-sill ratio (N/S). Shown are F values for the effects and the estimates of the error variances for cores and the residuals. F-values significant at 0.05, and 0.01 levels are marked with **, and ***, respectively.

Effect	Geostatistical parameter			
	Nugget	Sill	Range, mm	N/S
Land use system	0.7	1.0	3.1	2.8
Enzyme	11.8***	6.1***	1.5	5.6***
System*Enzyme	0.4	0.6	1.0	0.9
Core(Land use system) variance	93	409	0.1	9.4
Residual variance	162	1561	7.5	141

718

719 **Supplement Table 2.** Summary of pore-size distribution data obtained from μCT images with
720 scanning resolution of 29 μm.

Pore radius, μm	Pore volume, % of total			
	Mean	Standard deviation	Minimum	Maximum
30	0.17	0.09	0.05	0.42
60	0.69	0.38	0.22	2.01
90	0.78	0.48	0.17	2.60
120	0.49	0.33	0.08	1.67
150	0.45	0.32	0.06	1.53
180	0.23	0.16	0.03	0.75
210	0.21	0.15	0.02	0.68
240	0.13	0.09	0.01	0.40
270	0.12	0.08	0.01	0.36
300	0.08	0.06	0.01	0.28
330	1.82	1.38	0.06	6.45

721

References

Alef, K., Nannipieri, P., 1995. Cellulase activity, In: Alef, K., Nannipieri, P. (Eds.), Methods in applied soil microbiology and biochemistry. Academic, San Diego, CA, pp. 345–349.

Alef, K., Nannipieri, P., Trazar-Cepeda, C., 1995. Phosphatase activity, In: Alef, K., Nannipieri, P. (Eds.), Methods in applied soil microbiology and biochemistry. Academic, San Diego, CA, pp. 345–349.

Allison, S.D., 2005. Cheaters, diffusion and nutrients constrain decomposition by microbial enzymes in spatially structured environments. Ecology Letters 8, 626-635.

Athmann, M., Kautz, T., Banfield, C., Bauke, S., Hoang, D.T.T., Lusebrink, M., Pausch, J., Amelung, W., Kuzyakov, Y., Kopke, U., 2017. Six months of L-terrestris L. activity in root-formed biopores increases nutrient availability, microbial biomass and enzyme activity. Applied Soil Ecology 120, 135-142.

Bailey, V.L., A.P. Smith, M. Tfaily, S.J. Fansler, and B. Bond-Lamberty. 2017. Differences in soluble organic carbon chemistry in pore waters sampled from different pore size domains. Soil Biol. Biochem. 107:133-143. doi: 10.1016/j.soilbio.2016.11.025

Baldrian, P., 2014. Distribution of Extracellular Enzymes in Soils: Spatial Heterogeneity and Determining Factors at Various Scales. Soil Science Society of America Journal 78, 11-18.

Baldrian, P., Merhautova, V., Cajthaml, T., Petrankova, M., Snajdr, J., 2010a. Small-scale distribution of extracellular enzymes, fungal, and bacterial biomass in Quercus petraea forest topsoil. Biology and Fertility of Soils 46, 717-726.

Baldrian, P., Merhautova, V., Petrankova, M., Cajthaml, T., Snajdr, J., 2010b. Distribution of microbial biomass and activity of extracellular enzymes in a hardwood forest soil reflect soil moisture content. Applied Soil Ecology 46, 177-182.

Baldrian, P., Stursova, M., 2011. Enzymes in Forest Soils. Soil Enzymology 22, 61-73.

Baldrian, P., Vetrovsky, T., 2012. Scaling Down the Analysis of Environmental Processes: Monitoring Enzyme Activity in Natural Substrates on a Millimeter Resolution Scale. Applied and Environmental Microbiology 78, 3473-3475.

Banerjee, S., Bora, S., Thrall, P.H., Richardson, A.E., 2016. Soil C and N as causal factors of spatial variation in extracellular enzyme activity across grassland-woodland ecotones. Applied Soil Ecology 105, 1-8.

Banfield, C.C., Dippold, M.A., Pausch, J., Hoang, D.T.T., Kuzyakov, Y., 2017a. Biopore history determines the microbial community composition in subsoil hotspots. Biology and Fertility of Soils 53, 573-588.

Banfield, C.C., Zarebanadkouki, M., Kopka, B., Kuzyakov, Y., 2017b. Labelling plants in the Chernobyl way: A new Cs-137 and C-14 foliar application approach to investigate rhizodeposition and biopore reuse. Plant and Soil 417, 301-315.

Blagodatskaya, E., Kuzyakov, Y., 2008. Mechanisms of real and apparent priming effects and their dependence on soil microbial biomass and community structure: critical review. Biology and Fertility of Soils 45, 115-131.

763 Burns, R.G., 2013. Microbial Extracellular Enzymes and the Degradation of Natural and
764 Synthetic Polymers in Soil. Molecular Environmental Soil Science, 27-47.
765 Burns, R.G., DeForest, J.L., Marxsen, J., Sinsabaugh, R.L., Stromberger, M.E., Wallenstein,
766 M.D., Weintraub, M.N., Zoppini, A., 2013. Soil enzymes in a changing environment: Current
767 knowledge and future directions. Soil Biology & Biochemistry 58, 216-234.
768 Dick, W.A., Tabatabai, M.A., 1984. Kinetic-Parameters of Phosphatases in Soils and Organic
769 Waste Materials. Soil Science 137, 7-15.
770 Eivazi, F., Tabatabai, M.A., 1977. Phosphatases in Soils. Soil Biology & Biochemistry 9, 167-
771 172.
772 Franklin, R.B., Mills, A.L., 2009. Importance of spatially structured environmental heterogeneity
773 in controlling microbial community composition at small spatial scales in an agricultural field.
774 Soil Biology & Biochemistry 41, 1833-1840.
775 Ge, T.D., Wei, X.M., Razavi, B.S., Zhu, Z.K., Hu, Y.J., Kuzyakov, Y., Jones, D.L., Wu, J.S.,
776 2017. Stability and dynamics of enzyme activity patterns in the rice rhizosphere: Effects of plant
777 growth and temperature. Soil Biology & Biochemistry 113, 108-115.
778 German, D.P., Weintraub, M.N., Grandy, A.S., Lauber, C.L., Rinkes, Z.L., Allison, S.D., 2011.
779 Optimization of hydrolytic and oxidative enzyme methods for ecosystem studies. Soil Biology &
780 Biochemistry 43, 1387-1397.
781 Goovaerts, P., 1998. Geostatistical tools for characterizing the spatial variability of
782 microbiological and physico-chemical soil properties. Biology and Fertility of Soils 27, 315-334.
783 Guber, A., Kraychenko, A., Razavi, B.S., Uteau, D., Peth, S., Blagodatskaya, E., Kuzyakov, Y.,
784 2018. Quantitative soil zymography: Mechanisms, processes of substrate and enzyme diffusion
785 in porous media. Soil Biology & Biochemistry 127, 156-167.
786 Hapca, S., Baveye, P.C., Wilson, C., Lark, R.M., Otten, W., 2015. Three-Dimensional Mapping
787 of Soil Chemical Characteristics at Micrometric Scale by Combining 2D SEM-EDX Data and
788 3D X-Ray CT Images. Plos One 10.
789 Heitkotter, J., Marschner, B., 2018. Soil zymography as a powerful tool for exploring hotspots
790 and substrate limitation in undisturbed subsoil. Soil Biology & Biochemistry 124, 210-217.
791 Helliwell, J.R., Sturrock, C.J., Grayling, K.M., Tracy, S.R., Flavel, R.J., Young, I.M., Whalley,
792 W.R., Mooney, S.J., 2013. Applications of X-ray computed tomography for examining
793 biophysical interactions and structural development in soil systems: a review. European Journal
794 of Soil Science 64, 279-297.
795 Hoang, D.T.T., Pausch, J., Razavi, B.S., Kuzyakova, I., Banfield, C.C., Kuzyakov, Y., 2016a.
796 Hotspots of microbial activity induced by earthworm burrows, old root channels, and their
797 combination in subsoil. Biology and Fertility of Soils 52, 1105-1119.
798 Hoang, D.T.T., Razavi, B.S., Kuzyakov, Y., Blagodatskaya, E., 2016b. Earthworm burrows:
799 Kinetics and spatial distribution of enzymes of C-, N- and P- cycles. Soil Biology &
800 Biochemistry 99, 94-103.
801 Keiluweit, M., Gee, K., Denney, A., Fendorf, S., 2018. Anoxic microsites in upland soils
802 dominantly controlled by clay content. Soil Biology & Biochemistry 118, 42-50.
803 Keiluweit, M., Nico, P.S., Kleber, M., Fendorf, S., 2016. Are oxygen limitations under
804 recognized regulators of organic carbon turnover in upland soils? Biogeochemistry 127, 157-
805 171.

Keiluweit, M., Wanzek, T., Kleber, M., Nico, P., Fendorf, S., 2017. Anaerobic microsites have an unaccounted role in soil carbon stabilization. Nature Communications 8.
Ketcham, R.A., 2005. Three-dimensional grain fabric measurements using high-resolution X-ray computed tomography. Journal of Structural Geology 27, 1217-1228.
Kittler, J., Illingworth, J., 1986. Minimum Error Thresholding. Pattern Recognition 19, 41-47.
Kravchenko, A.N., Negassa, W., Guber, A.K., Schmidt, S., 2014. New Approach to Measure Soil Particulate Organic Matter in Intact Samples using X-Ray Computed Microtomography. Soil Science Society of America Journal 78, 1177-1185.
Kravchenko, A.N., Robertson, G.P., 2007. Can topographical and yield data substantially improve total soil carbon mapping by regression kriging? Agronomy Journal 99, 12-17.
Kuzyakov, Y., Razavi, B.S., 2019. Rhizosphere size and shape: Temporal dynamics and spatial stationarity. Soil Biology & Biochemistry (in press).
https://doi.org/10.1016/j.soilbio.2019.05.011
Liu, S.B., Razavi, B.S., Su, X., Maharjan, M., Zarebanadkouki, M., Blagodatskaya, E., Kuzyakov, Y., 2017. Spatio-temporal patterns of enzyme activities after manure application reflect mechanisms of niche differentiation between plants and microorganisms. Soil Biology & Biochemistry 112, 100-109.
Ma, X.M., Razavi, B.S., Holz, M., Blagodatskaya, E., Kuzyakov, Y., 2017. Warming increases hotspot areas of enzyme activity and shortens the duration of hot moments in the root-detritusphere. Soil Biology & Biochemistry 107, 226-233.
Malcolm, R.E., 1983. Assessment of Phosphatase-Activity in Soils. Soil Biology & Biochemistry 15, 403-408.
Mancarella, D.A., Basha, S.M.M., Mullins, D.E., Mansfield, E., Bazer, F.W., Roberts, R.M., 1981. Properties of a Membrane-Associated L-Leucine Beta-Naphthylamidase (Leucine Aminopeptidase) from the Porcine Uterus. Biology of Reproduction 24, 879-887.
Mganga, K.Z., Razavi, B.S., Kuzyakov, Y., 2016. Land use affects soil biochemical properties in Mt. Kilimanjaro region. Catena 141, 22-29.
Milliken, G.A., Johnson, D.E., 2001. Analysis of Messy Data Volume III: Analysis of covariance, 1st ed. CRC Press, Boca Raton, FL.
Milliken, G.A., Johnson, D.E., 2009. Analysis of Messy Data Volume I: Designed Experiments, 2nd ed. CRC Press.
Munch, B., Holzer, L., 2008. Contradicting Geometrical Concepts in Pore Size Analysis Attained with Electron Microscopy and Mercury Intrusion. Journal of the American Ceramic Society 91, 4059-4067.
Nakagawa, Y., Rosenfeld, A., 1979. Some Experiments on Variable Thresholding. Pattern Recognition 11, 191-204.
Nannipieri, P., Giagnoni, L., Renella, G., Puglisi, E., Ceccanti, B., Masciandaro, G., Fornasier, F., Moscatelli, M.C., Marinari, S., 2012. Soil enzymology: classical and molecular approaches. Biology and Fertility of Soils 48, 743-762.
Navratilova, D., Vetrovsky, T., Baldrian, P., 2017. Spatial heterogeneity of cellulolytic activity and fungal communities within individual decomposing Quercus petraea leaves. Fungal Ecology 27, 125-133.

Nunan, N., Ritz, K., Rivers, M., Feeney, D.S., Young, I.M., 2006. Investigating microbial micro-habitat structure using X-ray computed tomography. Geoderma 133, 398-407.
Nunan, N., Wu, K., Young, I.M., Crawford, J.W., Ritz, K., 2002. In situ spatial patterns of soil bacterial populations, mapped at multiple scales, in an arable soil. Microbial Ecology 44, 296-305.
Nunan, N., Wu, K.J., Young, I.M., Crawford, J.W., Ritz, K., 2003. Spatial distribution of bacterial communities and their relationships with the micro-architecture of soil. Fems Microbiology Ecology 44, 203-215.
Nye, P.H., Tinker, P.B., 1977. Solute Movement in the Soil-Root System. University of California Press, berkeley and Los Angeles, California.
Or, D., Smets, B.F., Wraith, J.M., Dechesne, A., Friedman, S.P., 2007. Physical constraints affecting bacterial habitats and activity in unsaturated porous media - a review. Advances in Water Resources 30, 1505-1527.
Pagliai, M., Denobili, M., 1993. Relationships between Soil Porosity, Root Development and Soil Enzyme-Activity in Cultivated Soils. Geoderma 56, 243-256.
Peth, S., 2010. Applications of Microtomography in Soils and Sediments, In: Balwant, S., Gräfe, M. (Eds.), Developments in Soil Science. Elsevier, The Netherlands, pp. 73-101.
Peth, S., Horn, R., Beckmann, F., Donath, T., Fischer, J., Smucker, A.J.M., 2008. Three-dimensional quantification of intra-aggregate pore-space features using synchrotron-radiation-based microtomography. Soil Science Society of America Journal 72, 897-907.
Probandt, D., Eickhorst, T., Ellrott, A., Amann, R., Knittel, K., 2018. Microbial life on a sand grain: from bulk sediment to single grains. Isme Journal 12, 623-633.
Quigley, M.Y., Negassa, W.C., Guber, A.K., Rivers, M.L., Kravchenko, A.N., 2018a. Influence of pore characteristics on the fate and distribution of newly added carbon Frontiers in Environmental Science 13.
Quigley, M.Y., Rivers, M.L., Kravchenko, A.N., 2018b. Patterns and sources of spatial heterogeneity in soil matrix from contrasting long term management practices. Frontiers in Environmental Science 29.
Rawlings, N.D., Tolle, D.P., Barrett, A.J., 2004. Evolutionary families of peptidase inhibitors. Biochemical Journal 378, 705-716.
Razavi, B.S., Blagodatskaya, E., Kuzyakov, Y., 2016. Temperature selects for static soil enzyme systems to maintain high catalytic efficiency. Soil Biology & Biochemistry 97, 15-22.
Razavi, B.S., Liu, S.B., Kuzyakov, Y., 2017. Hot experience for cold-adapted microorganisms: Temperature sensitivity of soil enzymes. Soil Biology & Biochemistry 105, 236-243.
Robertson, G.P., Hamilton, S.K., 2015. Long-term ecological research in agricultural landscapes at the Kellogg Biological Station LTER site: conceptual and experimental framework, In: Hamilton, S.K., Doll, J.E., Robertson, G.P. (Eds.), The ecology of agricultural landscapes: long-term research on the path to sustainability. Oxford University Press, New York, New York, USA., pp. 1-32.
Ruamps, L.S., Nunan, N., Chenu, C., 2011. Microbial biogeography at the soil pore scale. Soil Biology & Biochemistry 43, 280-286.

Ruamps, L.S., Nunan, N., Pouteau, V., Leloup, J., Raynaud, X., Roy, V., Chenu, C., 2013. Regulation of soil organic C mineralisation at the pore scale. Fems Microbiology Ecology 86, 26-35.
Sanaullah, M., Razavi, B.S., Blagodatskaya, E., Kuzyakov, Y., 2016. Spatial distribution and catalytic mechanisms of beta-glucosidase activity at the root-soil interface. Biology and Fertility of Soils 52, 505-514.
Schimel, J., Becerra, C.A., Blankinship, J., 2017. Estimating decay dynamics for enzyme activities in soils from different ecosystems. Soil Biology & Biochemistry 114, 5-11.
Schindelin, J., Arganda-Carreras, I., Frise, E., Kaynig, V., Longair, M., Pietzsch, T., Preibisch, S., Rueden, C., Saalfeld, S., Schmid, B., Tinevez, J.Y., White, D.J., Hartenstein, V., Eliceiri, K., Tomancak, P., Cardona, A., 2012. Fiji: an open-source platform for biological-image analysis. Nature Methods 9, 676-682.
Schmidt, H., Eickhorst, T., 2013. Spatio-temporal variability of microbial abundance and community structure in the puddled layer of a paddy soil cultivated with wetland rice (Oryza sativa L.). Applied Soil Ecology 72, 93-102.
Spohn, M., Kuzyakov, Y., 2014. Spatial and temporal dynamics of hotspots of enzyme activity in soil as affected by living and dead roots-a soil zymography analysis. Plant and Soil 379, 67-77.
Sprunger, C.D., Robertson, G.P., 2018. Early accumulation of active fraction soil carbon in newly established cellulosic biofuel systems. Geoderma 318, 42-51.
Strong, D.T., De Wever, H., Merckx, R., Recous, S., 2004. Spatial location of carbon decomposition in the soil pore system. European Journal of Soil Science 55, 739-750.
Stursova, M., Baldrian, P., 2011. Effects of soil properties and management on the activity of soil organic matter transforming enzymes and the quantification of soil-bound and free activity. Plant and Soil 338, 99-110.
Stursova, M., Barta, J., Santruckova, H., Baldrian, P., 2016. Small-scale spatial heterogeneity of ecosystem properties, microbial community composition and microbial activities in a temperate mountain forest soil. Fems Microbiology Ecology 92.
Tecon, R., Or, D., 2017. Biophysical processes supporting the diversity of microbial life in soil. Fems Microbiology Reviews 41, 599-623.
Wickings, K., Grandy, A.S., Kravchenko, A.N., 2015. Going with the flow: landscape position drives differences in microbial biomass and activity in conventional, low input, and organic agricultural systems in the Midwestern U.S. . Agriculture, Ecosystem and Environment 218, 1-10.
Young, I.M., Crawford, J.W., 2004. Interactions and self-organization in the soil-microbe complex. Science 304, 1634-1637.
Zhu, Q., Lin, H.S., 2010. Comparing Ordinary Kriging and Regression Kriging for Soil Properties in Contrasting Landscapes. Pedosphere 20, 594-606.